Performance analysis of source ranging by use of virtual receiver technique under different frequency bands *

YAO Meijuan[1,2,3] MA Li[1,2] LU Licheng[1,2] GUO Shengming[1,2]

(1 *Institute of Acoustics, Chinese Academy of Sciences* Beijing 100190)

(2 *Key Laboratory of Underwater Acoustics Environment, Chinese Academy of Sciences* Beijing 100190)

(3 *Chinese Academy of Sciences University* Beijing 100190)

Received Dec. 20, 2014

Revised Jan. 12, 2015

Abstract The traditional matched field processing localization need complicated computation to get the replica field and has high dependence on environment parameters and acoustic field model. To overcome the shortcoming, virtual receiver technique is used for source ranging. A virtual receiver is constructed by correlating the two signals of the guide source and the objective source received by a vertical line array. Then, the slope of the interference striation of the virtual receiver field is estimated using relevant signal processing method. Combining with the waveguide invariant β, the range of the objective source is determined. Through the numerical simulations and data processing collected from the experiment carried out in the South China Sea in 2004, the virtual receiver technique for broadband source ranging under the slope-bottom shallow water environment is discussed. As the frequency increases, the frequency bands should be broadened to obtain complete interference striation for good ranging results. In data processing, the receiving array spacing is too large to promise the orthogonality of the modes as the frequency increases and ranging results become worse.

PACS numbers: 43.30, 43.60

1 Introduction

Traditional matched field processing (Matched Field Processing, MFP) appeared in the late 1980s, which has been the focus of underwater acoustic research in the past few decades. Since Hinich[1] and Bucker[2] put forward the concept of matched field processing, the technology has made great progress in target detection and positioning, environmental parameters estimation, model algorithm evaluation and so on[3]. Matched field processing, which is based on field modeling, has high requirement on field modeling. Klemm[4] had already pointed out the mismatch problem in the early stages of his research work .At the same time, MFP, which is vulnerable to environment changes such as incomplete parameters measurement[5],changes of submarine topography[6], changes of sound velocity profile in time and space and differences of

* This work was supported by the National Natural Science Foundation of China (10774156).

the seabed sediment characteristics[7].Current domestic research on MFP technology research also focus on the influence of the environment mismatch[8−11]. Therefore, searching for a new localization method which don't need accurate priori knowledge of the environment has important significance.

The concept of virtual receiver is introduced in the late 1990s to underwater acoustics study. It can get the virtual field from the objective source in the guide source location through corresponding process of signals from the guide source and the objective source , thereby eliminating the effect of the environment changes between the vertical array and the guide source. Pierre D. Mourad[12] used the "Virtual" (Virtual receiver) concept to study the localization problem of the remote sound source at the low frequency and carried out the numerical simulation. Azmia. Al-Kurd and Robert P. Porter[13] concretely analyzed the performance of the holographic array processing algorithm (HAP). Martin Siderius[14]and others used the concept of virtual receiver to study multipath compensation in the shallow water environments. What's more, Aaron m. Thode[15] stepped further with his research work by using features of the shallow water waveguide invariant[16] to analyze different frequencies parts of broadband sources to achieve the purpose of ranging the target source.

The waveguide invariant (usually expressed as β) is an important quantity reflecting the interference structures of the sound field. In recent years, research on the waveguide invariant about objective range estimation and compensation of acoustic field spatial correlation has become a hotspot in underwater acoustics and provides a new way for sonar signal processing[17−19]. Traditional method to estimate the target range using the waveguide invariant is generally aimed at moving targets, by analyzing the interference stripes and its slope of LOFAR diagram and further estimate the target distance[20]. However, the method using virtual receive can estimate range of static(broadband) target sources without having to track the time course of the target motion.

Virtual receiver performance largely depends on whether the actual receiving array can well meet the orthogonality of the normal mode eigenfunction. Therefore, more strict requirements to the actual receiving vertical array aperture and array element spacing are put forward. Under different frequencies, the actual receiving array has different performances of normal mode sampling and the ranging results will also change. In this paper, ranging results are analyzed under different frequency bands through numerical simulation and experimental data processing. The second part briefly introduces the theory of the ranging method based on virtual receiving and the third part gives the results of numerical simulation. Then the following fourth part is the experimental data processing results. Finally the fifth part is the summary of the full text.

2 Method of object ranging based on virtual receiver technique

2.1 Virtual field

The vertical receiving array , the objective source and the guide source are placed as shown in Fig. 1. Consider that the water volume is horizontally uniform layered medium.

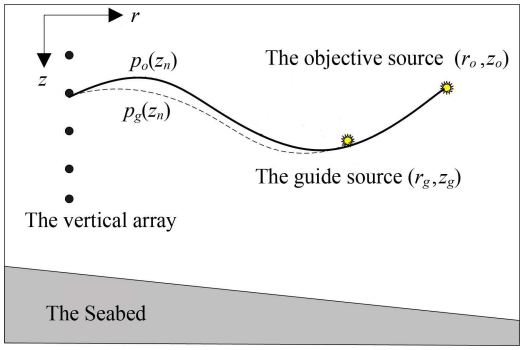

Fig. 1 Schematic of the shallow-water waveguide environment for virtual receive.

The signals received from the guide source and the target source should be divisible in time or by different SNR to ensure that the signal from the objective source and that from the guide source can be distinguished in the practical application. So the field from the objective source and the guide source that the nth element received are respectively:

$$P_{on} \equiv P_o(z_n, z_o, r_o, \omega) = S_o(\omega)\frac{1}{\rho_o}\sum_{\ell=1}^{M}\frac{\sqrt{2\pi}}{\sqrt{\xi_\ell r_o}}\psi_\ell(z_n)\psi_\ell(z_o)\mathrm{e}^{\mathrm{i}\xi_\ell r_o-\delta_\ell r_o+\mathrm{i}\pi/4}, \quad (1)$$

$$P_{gn} \equiv P_g(z_n, z_g, r_g, \omega) = S_g(\omega)\frac{1}{\rho_g}\sum_{\ell=1}^{M}\frac{\sqrt{2\pi}}{\sqrt{\xi_\ell r_g}}\psi_\ell(z_n)\psi_\ell(z_g)\mathrm{e}^{\mathrm{i}\xi_\ell r_g-\delta_\ell r_g+\mathrm{i}\pi/4}, \quad (2)$$

here z_o, z_g and z_n are respectively the depth of the objective source, the guide source and the n th element of the vertical array. ρ_o and ρ_g are respectively the density of the water volume where the objective source and the guide source are placed. ξ_ℓ, $\psi_\ell(z)$ and δ_ℓ are respectively the horizontal wave numbers, the eigenfunction and attenuation coefficients of the lth mode at radial frequency ω. $S_o(\omega)$ and $S_g(\omega)$ are the source spectrums.

The normalized virtual receiver output is given as follows:

$$\widetilde{V}(z_g, r_g, \omega_0; z_o, r_o, \omega_0) = \sum_{n=1}^{N} P_o^*(z_n, z_o, r_o, \omega_0)P_g(z_n, z_g, r_g, \omega_0), \quad (3)$$

here the asterisk mark notes complex conjugate. If we substitute Eq. (1) and Eq. (2) into Eq. (3), using the orthogonality of the normal modes:

$$\sum_{n=1}^{N}\psi_\ell(z_n, \omega_0)\psi_{\ell'}(z_n, \omega_0) \approx \delta_{\ell\ell'}, \quad (4)$$

we get:

$$V(z_g, r_g, \omega_0; z_o, r_o, \omega_0) = \sum_{\ell=1}^{M} N_\ell(r_o, r_g)\psi_\ell(z_o)\psi_\ell(z_g)\mathrm{e}^{\mathrm{i}\xi_\ell r_g-\mathrm{i}\xi_\ell r_o}, \quad (5)$$

here

$$N_\ell(r_o, r_g) = \frac{1}{\rho_o\rho_g}S_o(\omega_0)S_g(\omega_0)\frac{2\pi}{\xi_\ell\sqrt{r_o r_g}}\mathrm{e}^{-\delta_\ell(r_o+r_g)}, \quad (6)$$

Except for the magnitude of the sediment attenuation term and the extra factor in the denominator, Eq. (5) is similar to that of a receiver placed at the guide source location and can

be considered to be " virtual " acoustic field. Under the adiabatic approximation condition:

$$P_{on} \equiv P_o(z_n, z_o, r_o, \omega) \approx S_o(\omega)\frac{1}{\rho_o}\sum_{\ell=1}^{M}\frac{\sqrt{2\pi}}{\sqrt{W_\ell(r_o)}}\psi_\ell(z_n,0)\psi_\ell(z_o,\boldsymbol{r}_o)\mathrm{e}^{\mathrm{i}W_\ell(r_o)-U_\ell(r_o)+\mathrm{i}\pi/4}, \tag{7}$$

$$P_{gn} \equiv P_g(z_n, z_g, r_g, \omega) \approx S_g(\omega)\frac{1}{\rho_g}\sum_{\ell=1}^{M}\frac{\sqrt{2\pi}}{\sqrt{W_\ell(r_g)}}\psi_\ell(z_n,0)\psi_\ell(z_g,\boldsymbol{r}_g)\mathrm{e}^{\mathrm{i}W_\ell(r_g)-U_\ell(r_g)+\mathrm{i}\pi/4}, \tag{8}$$

here $\rho_o = \rho(z_o, \vec{r}_o)$ and $\rho_g = \rho(z_g, \vec{r}_g)$ are respectively the density of the water volume in the objective source and the guide source location. $\xi_\ell(\vec{r})$, $\psi_\ell(z, \vec{r})$ and $\delta_\ell(\vec{r})$ are respectively the eigenvalue, the eigenfunction and attenuation coefficient of the local mode.

$$W_\ell(r,\omega) = \int_0^r \xi_\ell(x,\omega)\mathrm{d}x,\ U_\ell(r,\omega) = \int_0^r \delta_\ell(x,\omega)\mathrm{d}x. \tag{9}$$

Also the virtual field is:

$$V(z_g, r_g, \omega_0; z_o, r_o, \omega_0) = \sum_{\ell=1}^{M} N_\ell(r_o, r_g)\psi_\ell(z_o,\boldsymbol{r}_o)\psi_\ell(z_g,\boldsymbol{r}_g)\mathrm{e}^{\mathrm{i}W_\ell(r_g)-\mathrm{i}W_\ell(r_o)}, \tag{10}$$

here

$$N_\ell(r_o, r_g) = \frac{1}{\rho_o\rho_g}S_o(\omega_0)S_g(\omega_0)\frac{2\pi}{\sqrt{U_\ell(r_o)U_\ell(r_g)}}\mathrm{e}^{-U_\ell(r_o)-U_\ell(r_g)}. \tag{11}$$

This expression is still similar to the field received at the guide source location from the objective source. Specially, when the environment between the guide source and the objective source is range independent:

$$V(z_g, r_g, \omega_0; z_o, r_o, \omega_0) = \sum_{\ell=1}^{M} N_\ell(r_o, r_g)\psi_\ell(z_o,\boldsymbol{r}_o)\psi_\ell(z_g,\boldsymbol{r}_g)\mathrm{e}^{\mathrm{i}\xi_{\ell g}(r_g-r_o)}, \tag{12}$$

here $\xi_{\ell g} = \xi_\ell(r_g) = \xi_\ell(r_o)$, $\psi_{\ell g}(z) = \psi_\ell(z, \vec{r}_g) = \psi_\ell(z, \vec{r}_o)$.

2.2 Object ranging

If the guide source location can be changed, ($r_g \to r_{g,i}$ or $z_g \to z_{g,i}$), then we can get a virtual field with a horizontal array or a vertical array. Based on this, it is not difficult to meditate corresponding matched field localization method or use the known guide source range r_g to estimate the unknown objective source range r_o. This method intend to avoid the effect from the horizontal inhomogeneous and time-varying environment parameters between the sources and the receiving array.

(1) Localization method 1

If the acoustic field of the broadband guide sound source and the target source and the subsequent virtual field is given, traditional matched field processing is not necessary actually. Analyzing the interference stripes can obtain the range of the object, just as the prevalent ranging method using the interference stripes. Intensity of the virtual field is:

$$I_V(r_o, z_o, \omega; r_g, z_g, \omega) \equiv |V|^2 = \sum_{m=1}^{M}\sum_{\ell=1}^{M} A_m^* A_\ell \cos\left\{\int_0^{r_g}\chi_{\ell m}(x,\omega)\mathrm{d}x - \int_0^{r_o}\chi_{\ell m}(x,\omega)\mathrm{d}x\right\}, \tag{13}$$

here,

$$\begin{cases} \chi_{\ell m}(r,\omega) \equiv \xi_\ell(r,\omega) - \xi_m(r,\omega), \\ A_\ell(\omega) \equiv N_\ell \psi_\ell(z_g, \boldsymbol{r}_g)\psi_\ell(z_o, \boldsymbol{r}_o). \end{cases} \tag{14}$$

To determine how contours of constant correlation in the virtual aperture output are related to the objective source range, the total differential of the virtual aperture output must be computed and set to zero:

$$\Delta I_V = \frac{\partial I_V}{\partial \omega}\Delta\omega + \frac{\partial I_V}{\partial r_g}\Delta r_g = 0. \tag{15}$$

When the amplitude varies little with the range and the frequency, we can get:

$$\frac{\partial I_V}{\partial \omega} \approx -\sum_{m=1}^{M}\sum_{\ell=1}^{M} A_m^* A_\ell \sin\left\{\int_0^{r_g} \chi_{\ell m}(x,\omega)\mathrm{d}x - \int_0^{r_o} \chi_{\ell m}(x,\omega)\mathrm{d}x\right\} \frac{\partial}{\partial \omega}\int_{r_o}^{r_g} \chi_{\ell m}(x,\omega)\mathrm{d}x, \tag{16}$$

$$\frac{\partial I_V}{\partial r_g} \approx -\sum_{m=1}^{M}\sum_{\ell=1}^{M} A_m^* A_\ell \sin\left\{\int_0^{r_g} \chi_{\ell m}(x,\omega)\mathrm{d}x - \int_0^{r_o} \chi_{\ell m}(x,\omega)\mathrm{d}x\right\} \frac{\partial}{\partial r_g}\int_{r_o}^{r_g} \chi_{\ell m}(x,\omega)\mathrm{d}x. \tag{17}$$

Note :

$$\int_0^r \chi_{\ell m}(x,\omega)\mathrm{d}x = \overline{\chi}_{\ell m}(r,\omega)r, \quad \overline{\chi}_{\ell m}(r,\omega) = \frac{1}{r}\int_0^r \chi_{\ell m}(x,\omega)\mathrm{d}x. \tag{18}$$

To be the average value of the wave number differences, there are

$$\frac{\partial}{\partial \omega}\int_{r_o}^{r_g} \chi_{\ell m}(x,\omega)\mathrm{d}x \approx (r_g - r_o)[\overline{S}_{g\ell}(r_g,\omega) - \overline{S}_{gm}(r_g,\omega)], \tag{19}$$

$$\frac{\partial}{\partial r_g}\int_{r_o}^{r_g} \chi_{\ell m}(x,\omega)\mathrm{d}x = \chi_{\ell m}(r_g,\omega) = \omega[S_{p\ell}(r_g,\omega) - S_{pm}(r_g,\omega)]. \tag{20}$$

So along a given stripe, there is

$$\frac{\Delta r_g}{\Delta\omega} = -\frac{r_g - r_o}{\omega}\frac{d\overline{S}_g(r_g)}{dS_p(r_g)} = -\frac{r_g - r_o}{\omega}\frac{1}{\beta(r_g)}, \quad \frac{r_g - r_o}{\omega} = \beta(r_g)\frac{\Delta r_g}{\Delta\omega}, \tag{21}$$

here

$$-\frac{d\overline{S}_g(r_g)}{dS_p(r_g)} = \frac{1}{\beta(r_g)}. \tag{22}$$

For the same stripe, considering the right side of equation (21) as a constant yields the final expression for the objective range:

$$r_o = r_{g1} - \beta\frac{r_{g2} - r_{g1}}{\omega_2 - \omega_1}\omega_1. \tag{23}$$

(2) Localization method 2

The localization method above can be further simplified using the broadband guide source. One can compute a new quantity of the virtual receive form:

$$I_V(r_o, z_o, \omega; r_g, z_g, \omega') \equiv |V|^2 = \sum_{m=1}^{M}\sum_{\ell=1}^{M} A_m^* A_\ell \cos\left\{\int_0^{r_g} \chi_{\ell m}(x,\omega)\mathrm{d}x - \int_0^{r_o} \chi_{\ell m}(x,\omega')\mathrm{d}x\right\}. \tag{24}$$

Under the adiabatic approximation condition, the expression for $\beta^{-1}(r)$ is[21]:

$$\frac{1}{\beta(r)} = -\frac{\omega}{r}\frac{1}{\chi_{\ell m}(0,\omega)}\int_0^r \frac{\partial \chi_{\ell m}(x,\omega)}{\partial \omega}\mathrm{d}x. \tag{25}$$

The relationship between the horizontal wave number differences and the waveguide invariant[22] is:

$$\chi_{\ell m}(r,\omega) = C_{\ell m}(r)\omega^{-1/\beta(r)}. \tag{26}$$

Substitute Eq. (26) into Eq. (25), there is:

$$\int_0^r \chi_{\ell m}(x,\omega)\mathrm{d}x = r\frac{\beta(0)}{\beta(r)}\chi_{\ell m}(0,\omega). \tag{27}$$

Substituting Eq. (27) into Eq. (24) yields the expression of the intensity:

$$I_V(r_o,z_o,\omega;r_g,z_g,0) = \sum_{m=1}^{M}\sum_{\ell=1}^{M} A_m^* A_\ell \cos\left\{\left(\frac{\beta(0)}{\beta(r_o)}r_o - \frac{\beta(0)}{\beta(r_g)}r_g\right)\chi_{\ell m}(0,\omega)\right\}, \tag{28}$$

$$I_V(r_o,z_o,\omega;r_g,z_g,\omega') = \sum_{m=1}^{M}\sum_{\ell=1}^{M} A_m^* A_\ell \cos\left\{\left(\frac{\beta(0)}{\beta(r_o)}r_o - \frac{\beta(0)}{\beta(r_g)}r_g\left(1+\frac{\omega_s}{\omega}\right)^{-1/\beta(0)}\right)\chi_{\ell m}(0,\omega)\right\}. \tag{29}$$

The slope of the lines of constant correlation is:

$$\left(\frac{\Delta\omega_s}{\Delta\omega}\right)_{\text{contour}} \equiv \kappa = -\frac{\partial I_V/\partial\omega}{\partial I_V/\partial\omega_s}. \tag{30}$$

Further derivation yields the final expression of the object range:

$$r_o = r_g\frac{\beta(r_o)(1+\kappa)}{\beta(r_g)(1+\omega_s/\omega)^{1+1/\beta(0)}} \approx r_g\frac{\beta(r_o)(1+\kappa)}{\beta(r_g)}. \tag{31}$$

When the sea depth varies linearly, β can be approximated as[23] :

$$\frac{\beta(r_o)}{\beta(r_g)} = \frac{D(r_o)}{D(r_g)}, \tag{32}$$

here D is the sea depth, so another expression of the object range is:

$$r_o = r_g\frac{D(r_o)}{D(r_g)}(1+\kappa). \tag{33}$$

Eq. (33) is an iterative solution in the form.

3 Numerical simulations

Schematic of the shallow-water waveguide environment is shown as Fig. 2. The sea depth varies linearly from 80 m to 100 m while the distance varies from 30 km to 100 km. 40 elements of the vertical array are distributed in the water volume from 2 m depth to 80 m depth.

The Submarine medium is considered homogeneous and semi-infinite. The sound speed profile and the submarine medium parameters are shown as Fig. 2. We can analyze the problems under the adiabatic approximation condition for the slope is light.

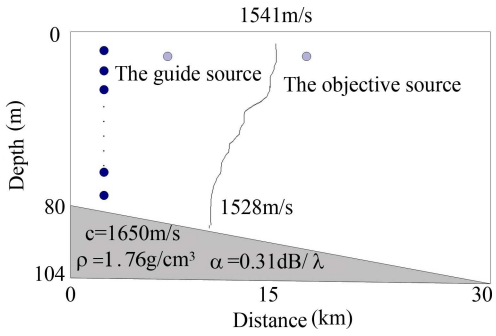

Fig. 2 Sketch of the underwater environment for simulation.

The guide source is applied at 7 m depth and 12 km range while the objective source is applied at 7 m depth and 18 km range. Ranging results under different frequency bands are shown in Fig.3. Fig. 3(a) is the ranging result under the frequency band of 80–140 Hz with the left one being interference stripes of the virtual field, the middle one being the Radon transform of the interference stripes and the right one being the standard deviation of radon transform. Note θ to be the angle between the stripes and the positive direction of X axis. So the relationship between the angle θ and the slope of the stripes is presented as the following Eq. (34). The standard deviation provides a rough measure of the angle and the angle can be inverted into a hypothetical test range using Eq. (33).

$$\tan\theta = \frac{\Delta\omega}{\Delta\omega_s} = \frac{1}{\kappa}. \tag{34}$$

Fig. 3(b) is the ranging result under the frequency band 130–190 Hz. Both Fig. 3(a) and Fig. 3(b) present clear interference stripes and give good ranging results as 17.41 km and 17.56 km respectively with the corresponding error 3.28% and 1.6%. Fig. 3(c) is the ranging result under the higher frequency band 180–240 Hz and the ranging results is 16.54 km with a more obvious error 8.11% than the previous two figures. Compare Fig. 3(a), Fig. 3(b) and Fig. 3(c), it is easy to see that as the frequency increases, the interference stripes tends to be wider, which can be explained as follows (L.M.Brekhovskikh, "Fundamentals of Ocean Acoustics," p160): for low-order normal modes (small grazing angle conditions) meeting the conditions that the quantity $[(l+0.5)\pi/(kh)]^2$ is far less than 1, there is:

$$\chi_{lm} = \frac{\pi^2 c}{2h^2}\left[\left(m+\frac{1}{2}\right)^2 - \left(l+\frac{1}{2}\right)^2\right]\frac{1}{\omega}. \tag{35}$$

Suppose that other conditions are unchanged, with the frequency increasing, the horizontal wave number differences become smaller. So the stripes interval becomes wider.

In view of the interference stripes interval becoming wider with frequency increasing, the frequency bands should be broadened to get complete and clear interference stripes, broadening the frequency bands to 180–300 Hz can get more clear interference stripes presented as Fig. 3(d) with the ranging results 17.71 km and the ranging error 1.61% .To ensure that the interference stripes are clear and complete is the premise of obtaining correct ranging results.

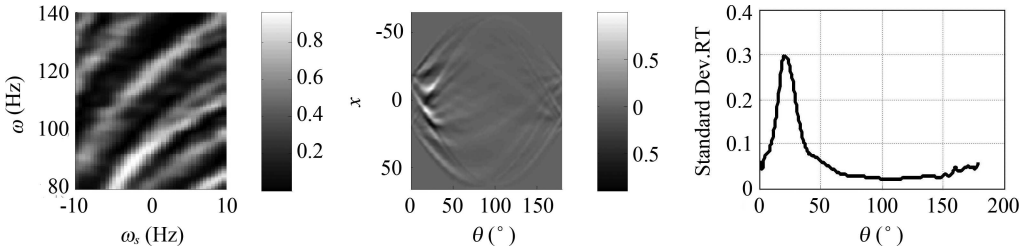

(a) The estimating result is that $\theta = 21°$, and ranging result is 17.41 km.

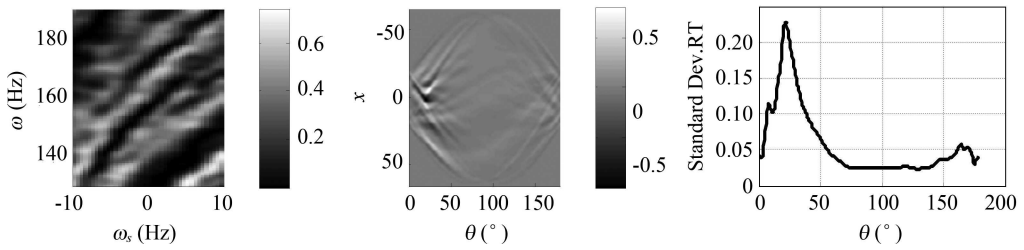

(b) The estimating result is that $\theta = 21.5°$, and ranging result is 17.56 km.

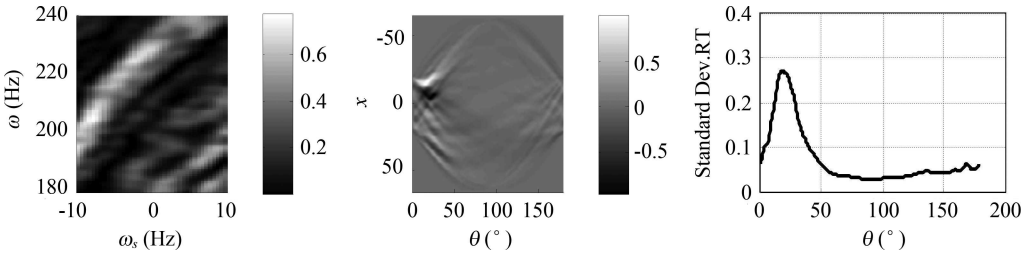

(c) The estimating result is that $\theta = 18°$, and ranging result is 16.54 km.

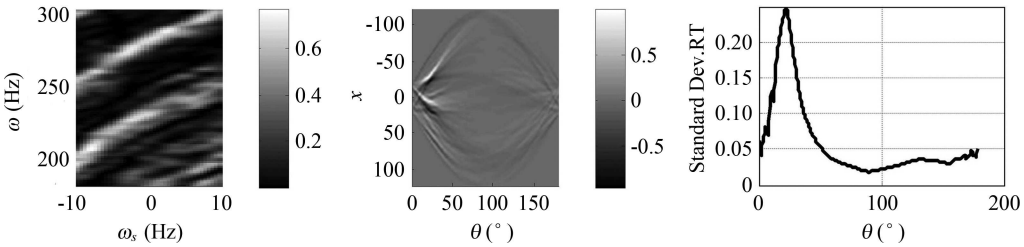

(d) The estimating result is that $\theta = 20°$, and ranging result is 17.11 km.

Fig. 3 Simulation ranging results with complete array under different frequency bands.

4 Experiment data processing and analysis

The experimental data is explosion data from South Sea in 2004. The sound speed profile and submarine topography are shown as Fig. 4 and Fig. 5.

32 elements of the vertical array are uniformly distributed in 2–64 m depth of the water volume. Because some elements of the array failed to record the signal, the actual number of the elements is 18. The corresponding depth of the elements is [6 10 12 14 16 26 32 36 38 46 48 50 58 60 62 64]. The guide source is applied at 7 m depth and 12.20 km range while the actual position of the objective source is 7 m depth and 17.94 km range.

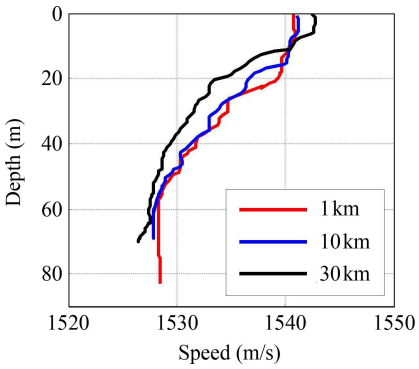

Fig. 4 The sound speed profile.

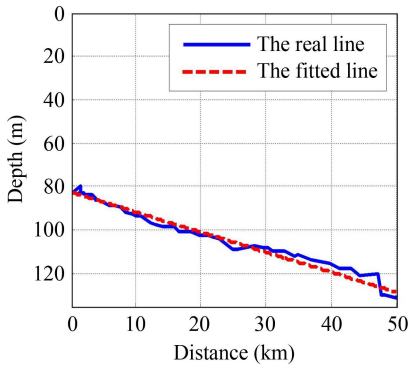

Fig. 5 The submarine topography.

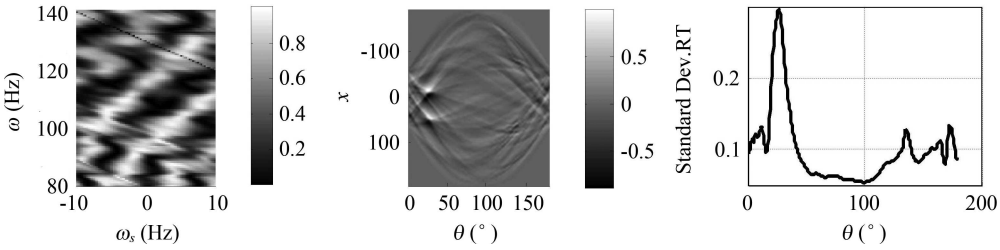

(a) The estimating result is that $\theta = 26°$, and ranging result is 19.43 km.

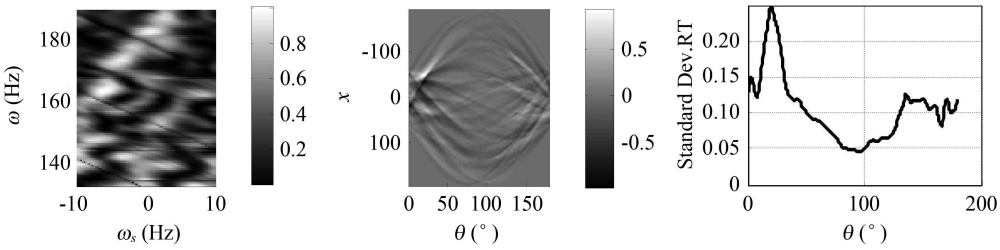

(b) The estimating result is that $\theta = 19.5°$, and ranging result is 17.53 km.

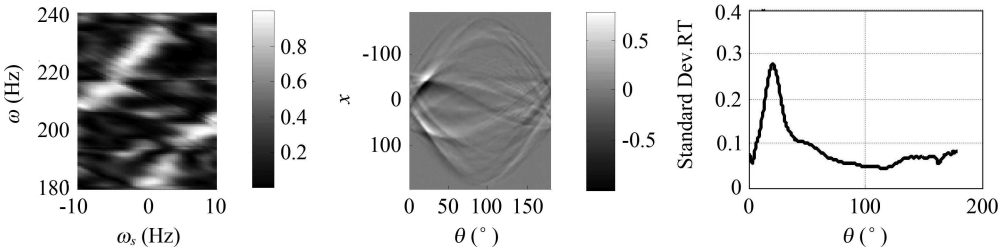

(c) The estimating result is that $\theta = 21°$, and ranging result is 17.81 km.

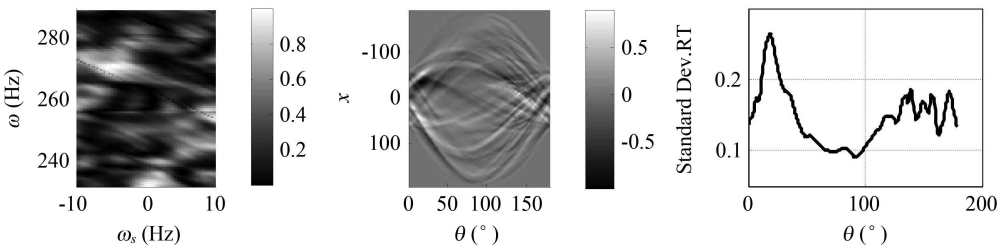

(d) The estimating result is that $\theta = 18.5°$, and ranging result is 17.06 km.

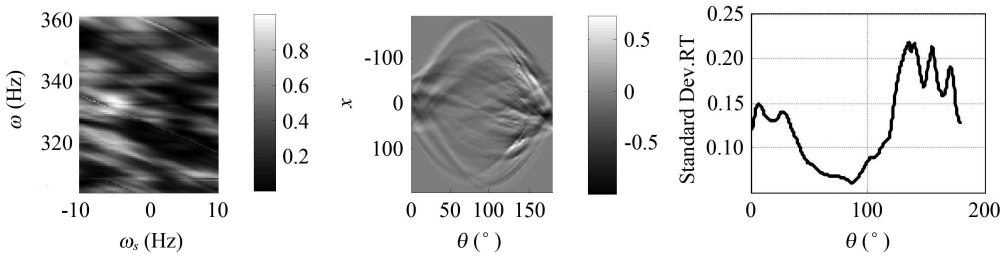

(e) The estimating result is that $\theta = 135°$, and ranging result is 0 km.

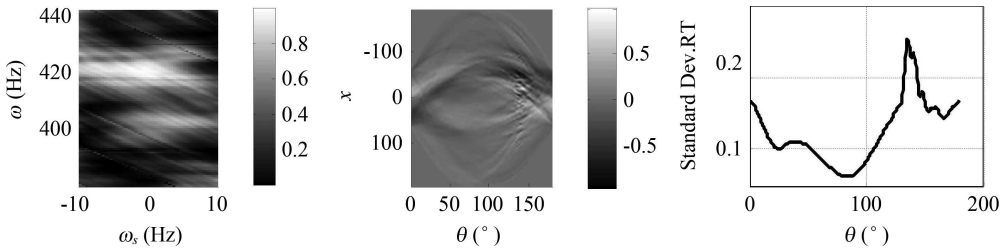

(f) The estimating result is that $\theta = 135.5°$, and ranging result is 0.19 km.

Fig. 6 Experiment ranging results with incomplete array under different frequency bands.

Table 1 Ranging results of the other two groups (km)

Group number \ Frequency bands (Hz)	80–140	130–190	180–240	230–290	280–340
1	10.93	10.84	10.67	0.47	0.59
2	23.37	21.46	22.92	22.92	4.92

It is clear that the interference stripes interval becomes wider with the frequency increasing, which is sealed with the results of numerical simulation. Figs. 6(a)–(d) are respectively the ranging results under the frequency bands 80–140 Hz, 130–190 Hz, 180–240 Hz and 230–290 Hz. The ranging results are respectively 19.43 km, 17.35 km, 17.81 km, 17.81 km, with the corresponding ranging error 8.31%, 3.29%, 0.72%, 3.29%. The ranging results are good since the ranging errors are all less than 10%.

Ensuring the integrity of the normal modes is the prerequisite of virtual receive. The sampling performance of the normal modes under different frequencies is different. When the orthogonality of normal modes is broken, extra interfere will be introduced to Eq. (5) to give inaccurate ranging results. One can also see that there are other local extremes besides the maximum radon standard deviation curve. Further, with the frequency increasing, the maximum of the curve appears at 135° as shown in Figs. 6(e)–(f). The other two groups of ranging results are shown in Table 1. The guide source is positioned at 7.58-km range while the objective source is positioned at 11.27-km range in the first group. And the guide source is positioned at 12.20-km range while the objective source is positioned at 21.40-km range. Under the lower frequency bands both the two groups give good ranging results, however, under the higher frequency bands the results become inaccurate.

In order to better analyze and illustrate the importance of the integrity of the normal modes sampling in ranging using virtual receiver technique, another simulation with the same

distributed array as the experiment is analyzed. The ranging results are shown in Fig. 7.

Figs. 7(a)–(d) are respectively the ranging results under the same frequency bands as Figs. 3(a)–(d). The interference stripes in Fig. 7 are not so regular as that in Fig. 3.

Also, there are other local extremes in the standard deviation curve besides the maximum, which is the similar phenomenon appearing in the experiment data processing. What's more, with the frequency increasing, the local extreme appearing becomes more clear shown as Figs. 7(e)–(f). The reason for this phenomenon is that the orthogonality of the normal modes is broken by incomplete sampling. Considering Eq. (28) and Eq. (29), Assume that the field from the guide source and that from the objective source is destroyed at frequency ω, then the virtual field $I_{V1}(r_o, z_o, \omega; r_g, z_g, \omega)$, $I_{V2}(r_o, z_o, \omega - \omega_s; r_g, z_g, \omega)$, $I_{V3}(r_o, z_o, \omega + \omega_s; r_g, z_g, \omega)$ will

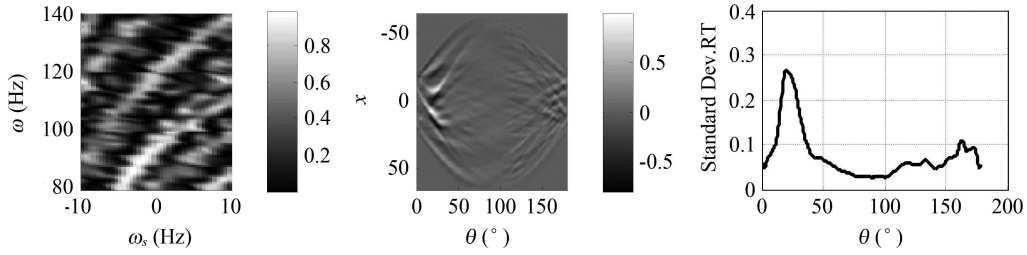

(a) The estimating result is that $\theta = 20.5°$, and ranging result is 17.26 km.

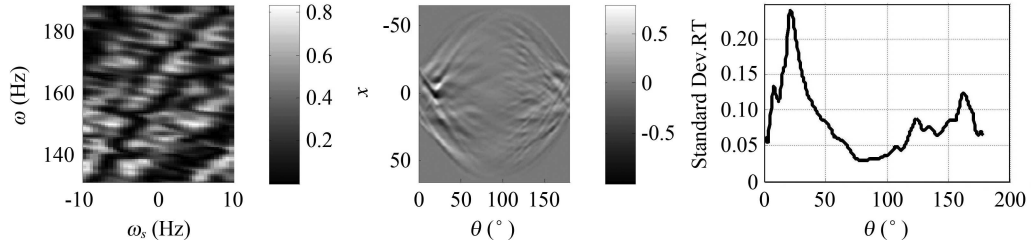

(b) The estimating result is that $\theta = 21.5°$, and ranging result is 17.56 km.

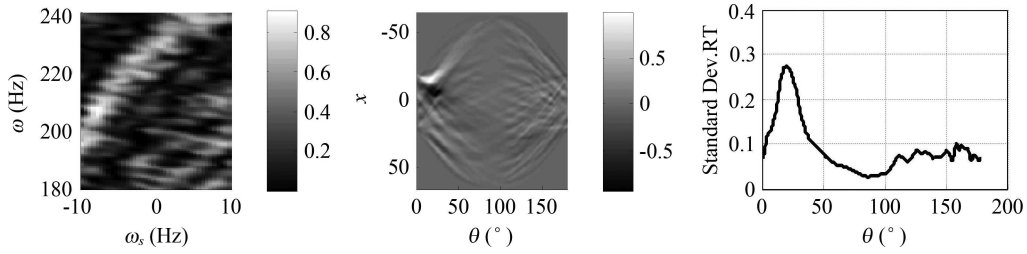

(c) The estimating result is that $\theta = 20.5°$, and ranging result is 17.26 km.

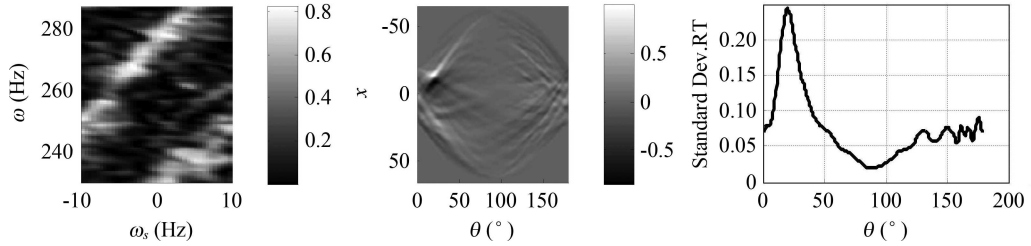

(d) The estimating result is that $\theta = 20°$, and ranging result is 17.11 km.

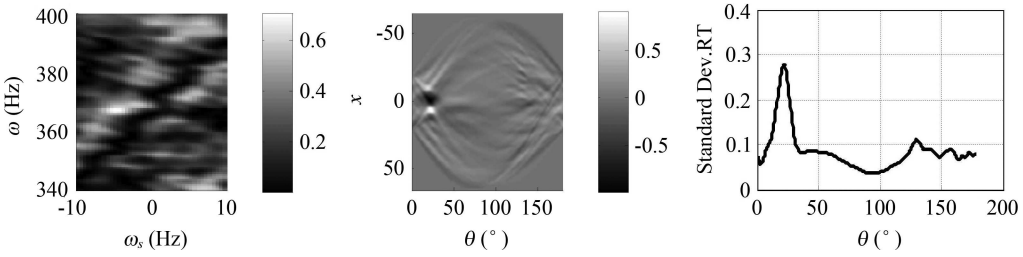

(e) The estimating result is that $\theta = 21.5°$, and ranging result is 17.56 km.

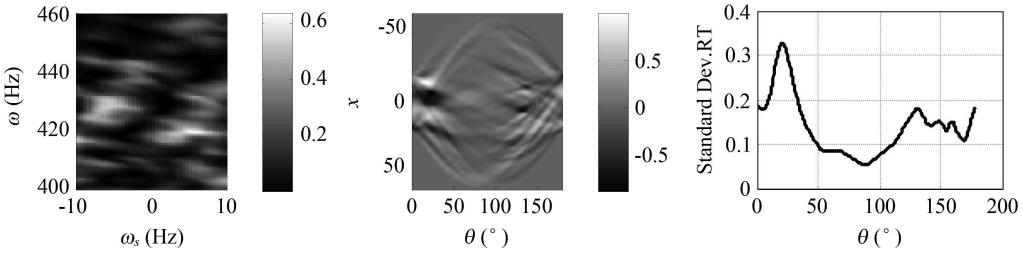

(f) The estimating result is that $\theta = 21°$, and ranging result is 17.41 km.

Fig. 7 Simulation ranging results with incomplete array under different frequency bands.

be destroyed too. As a consequence, the points which are interfered can form some stripes. One can calculate the slope by the following Equations:

Slope of the stripes formed by I_{V1}, I_{V2}:

$$\kappa = \left(\frac{\Delta\omega_s}{\Delta\omega}\right)_{1,2} = \frac{[\omega - (\omega - \omega_s)] - (\omega - \omega)}{(\omega - \omega_s) - (\omega)} = -1, \tag{36}$$

Slope of the stripes formed byI_{V1}, I_{V3}:

$$\kappa = \left(\frac{\Delta\omega_s}{\Delta\omega}\right)_{1,3} = \frac{[\omega - (\omega + \omega_s)] - (\omega - \omega)}{(\omega + \omega_s) - (\omega)} = -1, \tag{37}$$

Slope of the stripes formed byI_{V2}, I_{V3}:

$$\kappa = \left(\frac{\Delta\omega_s}{\Delta\omega}\right)_{2,3} = \frac{[\omega - (\omega + \omega_s)] - [\omega - (\omega - \omega_s)]}{(\omega + \omega_s) - (\omega - \omega_s)} = -1. \tag{38}$$

One can know that by Eq. (34), when the slope of stripes is -1 just like Eqs. (36)–(38) , the maximum of the standard deviation appears at the point where the corresponding angle must be 135°.

Therefore, under the higher frequency bands, shown as Figs. 6(e)–(f), the orthogonality of the normal modes is seriously destroyed to give bad ranging results. To ensure accurate ranging results, the interval between the adjacent two elements shouldn't be larger than half of the wavelength.

5 Conclusion

Source ranging using virtual receiver method can avoid field modeling and complex field calculation and need little prior knowledge of the environment. Through numerical simulation and analysis of experimental data processing, source ranging results using virtual receiver

method under different frequency bands are given and analyzed. The following conclusions are confirmed. First, source ranging results are satisfactory under the lower frequency bands with appropriate vertical array. Second, with the frequency increasing, the frequency bands should be broadened to get clear and complete interference stripes. Third, the requirement for the vertical array is higher with the frequency increasing. Under the lower frequency bands good ranging results through experiment data processing is presented while under the higher frequency bands bad ranging results is presented with incomplete vertical array.

References

[1] Hinich M J. Maximum Likelihood Signal Processing for a Vertical Array. *J. Acoust. Soc. Am.*, 1973; **54**(2): 499–503

[2] Bucker H P. Use of Calculated Sound Fields and Matched-field Detection to Locate Sound Sources in Shallow Water. *J. Acoust. Soc. Am.*, 1976; **59**(2): 368–373

[3] Baggeroer, Kuperman W A, Milkhalevsky P N. An overview of matched field methods in ocean acoustics. *IEEE J. Oceanic Eng.*, 1993; **18**(4): 401–424

[4] Klemm R. Range and depth estimation by line arrays in shallow water. *Signal Processing*, 1981(3): 333–314

[5] Shang E C, Wang Y Y. Environmental mismatching effects on source localization processing in mode space. *J. Acoust. Soc. Am.*, 1991; **89**(5): 2285–2290

[6] Li Zhenglin, Zhang Renhe, Yan Jin, Peng Zhaohui, Li Fenghua. Broadband matched-field source localization in the continental slope environment. *Journal of Acoustics*(in Chinese), 2003; **28**(5): 425–428

[7] Donald R, Del Balzo, Christopher Feuillade, Mary M Row. Effects of water-depth mismatch on matched-field localization in shallow water. *J. Acoust. Soc. Am.*, 1988; **83**(6): 2180–2185

[8] Yang Kunde, Ma Yuanliang,Zou Shixin, Lei Bo. Linear matched field processing based on environmental perturbation. *Journal of Acoustics*(in Chinese), 2006; **31**(6): 496–505

[9] Yang Kunde, Ma Yuanliang, Zhang Zhongbing, Zou Shixin. Robust adaptive matched field processing with environmental uncertainty. *Chinese Journal Acoustics*, 2006; **25**(2): 159–170

[10] Li Jianlong, Pan Xiang. A Bayesian approach to matched field processing in untertain ocean environments. *Journal of Acoustics*(in Chinese), 2008; **33**(3): 205–211

[11] Yang Kunde, Ma Yuanliang. Robust adaptive matched field processing with sector eigenvector constraints. *Chinese Journal Acoustics*, 2006; **25**(3): 243–257

[12] Mourad P D, Rouseff D, Porter R P, Al-Kurd A. Source localization using a reference wave to correct for oceanic variability. *J. Acoust. Soc. Am.*, **92**(2): 1031–1039

[13] Al-Kurd A A, Porter R P. Performance analysis of the holographic array processing algorithm. *J. Acoust. Soc. Am.*, 1995; **97**(3): 1747–1761

[14] Siderius M, Jackson D R, Rouseff D, Porter R. Multipath compensation in shallow water environments using a virtual receiver. *J. Acoust. Soc. Am.*, 1997; **102**(6): 3439–3449

[15] Thode A M. Souce ranging with minimal environmental information using a virtual receiver and waveguide invariant theory. *J. Acoust. Soc. Am.*, 2000; **108**(4): 1582–1594

[16] Hodgkiss W S, Song H C, Kuperman W A. A long-range and variable focus phase-conjugation experiment in shallow water. *J. Acoust. Soc. Am.*, 1999; **105**(3): 1594–1604

[17] Yu Yun, Hui Junying. Passive ranging based on acoustic field interference structure using double arrays (elements. *Chinese Journal Acoustics*, 2012; **31**(3): 262–274

[18] Guo Guoqiang, Yang Yixin, Sun Chao, Li Bo. Waveguide invariance structure for low frequency monostatic bottom reverberation mitigation in shallow water. *Chinese Journal Acoustics*, 2011; **30**(1): 81–94

[19] Su Xiaoxing, Zhang Renhe, Li Fenghua, Improvement of the longitudinal correlations of acoustical field by using the waveguide invariance. *Journal of Acoustics*(in Chinese), 2006; **31**(4): 305–309

[20] Yu yun, Hui Junying, Yin Jingwei, Hui juan, Wang Zijuan. Moving target parameter estimation and passive ranging based on waveguide invariant theory. *Journal of Acoustics*(in Chinese), 2011; **36**(3): 258–264

[21] Chuprov S D. Interference structure of a sound field in a layered ocean. *Ocean Acoustics*, 1982: 71–91

[22] Grachev G A. Theory of acoustic field invariants in layered waveguide. *Acoust. Phys.*, 1994; **39**: 33–35

[23] D'Spain G L, Kuperman W A. Application of waveguide invariants to analysis of spectrograms from shallow water environments that vary in range and azimuth. *J. Acoust. Soc. Am.*, 1999; **106**(5): 2454–2468